Electronic Supplementary Material (ESI) for Physical Chemistry Chemical Physics.

Supplementary Information

Nanoparticle-induced ion-sensitive reduction in decane-water interfacial tension

Boyao Wen, Chengzhen Sun, Bofeng Bai*

State Key Laboratory of Multiphase Flow in Power Engineering, Xi'an Jiaotong University, Xi'an, Shaanxi, 710049, China.

* Corresponding Author. Tel: +86-029-82665316; Electronic mail: bfbai@mail.xjtu.edu.cn

Contents

1. Model and methods

1.1 Interaction potentials

1.1.1 OPLS All-Atom force field

In our work, we employ the OPLS All-Atom (OPLS-AA) force field [1] to describe the interactions between decane molecules, which can accurately regenerate the thermodynamic properties of organic liquids. This force field includes non-bonded interactions, bond stretching, angle bending and torsion interactions:

$$E = E_{ab} + E_{bond} + E_{angle} + E(\phi) \tag{S1}$$

The non-bonded interaction contains the standard Lennard-Jones and Coulombic pairwise interactions, given by

$$E_{ab} = 4\varepsilon\left[\left(\frac{\sigma}{r_{ab}}\right)^{12} - \left(\frac{\sigma}{r_{ab}}\right)^{6}\right] + \frac{Cq_aq_b}{\chi r_{ab}} \qquad (r_{ab} < r_{cut}) \tag{S2}$$

where ε is the potential well depth, σ the distance at which the potential is zero, r_{cut} the cut-off radius, C an energy-conversion constant, q_a and q_b the charges of atom a and b, and χ is the dielectric constant. While r_{ab} is greater than r_{cut}, the long-range electrostatic interactions are described by Particle-Particle Particle-Mesh (PPPM) method. Potential parameters between the crossing atoms are obtained based on the Lorentz-Berthelot mixing rule,

$$\sigma_{ij} = \frac{\sigma_{ii} + \sigma_{jj}}{2} \qquad \varepsilon_{ij} = \sqrt{\varepsilon_{ii}\varepsilon_{jj}} \tag{S3}$$

All the LJ potential parameters are listed in **Table S1**.

Table S1. LJ potential parameters used in the simulations.

Type	ε (eV)	σ (Å)
O-O	6.591×10^{-3}	3.1507
H(H_2O)-H(H_2O)	1.995×10^{-3}	0.4000
C-C	2.862×10^{-3}	3.5000
H(Decane)-H(Decane)	1.301×10^{-3}	2.5000
Si-Si	4.033×10^{-3}	4.1500

$O(SiO_2)$-$O(SiO_2)$	2.342×10^{-3}	3.4700
$H(SiO_2)$-$H(SiO_2)$	1.301×10^{-3}	2.5000
Na-Na	5.640×10^{-3}	2.3500
Ca-Ca	19.501×10^{-3}	2.3609
Mg-Mg	37.944×10^{-3}	1.3976
Cl-Cl	4.341×10^{-3}	4.4015
O-$H(H_2O)$	3.364×10^{-3}	1.7753
O-C	4.351×10^{-3}	3.3254
O-H(Decane)	2.934×10^{-3}	2.8254
O-Si	5.156×10^{-3}	3.6504
O-$O(SiO_2)$	5.905×10^{-3}	3.3104
O-$H(SiO_2)$	2.928×10^{-3}	2.8254
O-Na	6.097×10^{-3}	2.7504
O-Ca	11.337×10^{-3}	2.7558
O-Mg	15.814×10^{-3}	2.2742
O-Cl	5.349×10^{-3}	3.7761
$H(H_2O)$-C	2.393×10^{-3}	1.9500
$H(H_2O)$-H(Decane)	1.613×10^{-3}	1.4500
$H(H_2O)$-Si	2.836×10^{-3}	2.2750
$H(H_2O)$-$O(SiO_2)$	3.249×10^{-3}	1.9350
$H(H_2O)$-$H(SiO_2)$	1.611×10^{-3}	1.4500
$H(H_2O)$-Na	3.354×10^{-3}	1.3750
$H(H_2O)$-Ca	6.237×10^{-3}	1.3805
$H(H_2O)$-Mg	8.700×10^{-3}	0.8988
$H(H_2O)$-Cl	2.943×10^{-3}	2.4008
C-H(Decane)	1.931×10^{-3}	3.0000
C-Si	3.397×10^{-3}	3.8250
C-$O(SiO_2)$	3.891×10^{-3}	3.4850
C-$H(SiO_2)$	1.930×10^{-3}	3.0000
C-Na	4.018×10^{-3}	2.9250
C-Ca	7.471×10^{-3}	2.9305

C-Mg	10.421 ×10^{-3}	2.4488
C-Cl	3.525 ×10^{-3}	3.9508
H(Decane)-Si	2.290 ×10^{-3}	3.3250
H(Decane)-O(SiO_2)	2.623 ×10^{-3}	2.9850
H(Decane)-H(SiO_2)	1.301 ×10^{-3}	2.5000
H(Decane)-Na	2.709 ×10^{-3}	2.4250
H(Decane)-Ca	5.037 ×10^{-3}	2.4305
H(Decane)-Mg	7.026 ×10^{-3}	1.9488
H(Decane)-Cl	2.376 ×10^{-3}	3.4508
Si-O(SiO_2)	4.619 ×10^{-3}	3.8100
Si-H(SiO_2)	2.291 ×10^{-3}	3.3250
Si-Na	4.769 ×10^{-3}	3.2500
Si-Ca	8.868 ×10^{-3}	3.2555
Si-Mg	12.370 ×10^{-3}	2.7738
Si-Cl	4.184 ×10^{-3}	4.2758
O(SiO2)-H(SiO_2)	1.746 ×10^{-3}	2.9850
O(SiO2)-Na	3.634 ×10^{-3}	2.9100
O(SiO2)-Ca	6.758 ×10^{-3}	2.9155
O(SiO2)-Mg	9.427 ×10^{-3}	2.4338
O(SiO2)-Cl	3.189 ×10^{-3}	3.9358
H(SiO_2)-Na	2.709 ×10^{-3}	2.4250
H(SiO_2)-Ca	5.037 ×10^{-3}	2.4305
H(SiO_2)-Mg	7.026 ×10^{-3}	1.9488
H(SiO_2)-Cl	2.376 ×10^{-3}	3.4508
Na-Cl	4.948 ×10^{-3}	3.3758
Ca-Cl	9.201 ×10^{-3}	3.3811
Mg-Cl	12.834 ×10^{-3}	2.8996

The bond stretching and angle bending in the molecules and silica nanoparticles are described by the *harmonic* potential as follows,

$$E_{bond} = K_{bond}(r_{ab} - r_0)^2 \quad \text{(S4)}$$

$$E_{angle} = K_{angle}(\theta - \theta_0)^2 \quad \text{(S5)}$$

where K_{bond} *and* K_{angle} are the bond and angle coefficients concerning with energy, r_0 is the equilibrium bond distance, and θ_0 is the equilibrium bond angle. All bond and angle potential coefficients are shown in **Table S2**.

Table S2. Bond stretching and angle bending parameters.

Type	r_0 (Å) or θ_0 (°)	K_{bond} or K_{angle} (eV)
O-H (water)	0.9572	19.514
C-H	1.0900	14.744
C-C	1.5290	11.622
O-Si	1.6800	12.358
O-H (SiO_2)	0.9450	21.463
H-Si	1.3820	8.027
H-O-H	104.52	2.385
H-C-H	107.80	1.431
C-C-H	110.70	1.626
C-C-C	109.50	2.530
O-Si-O (inside)	109.47	3.349
O-Si-O (surface)	113.10	1.834
Si-O-Si	149.80	1.349
Si-O-H	115.00	2.168
O-Si-H	113.40	1.444
H-Si-H	112.00	1.379

The last term of the OPLS-AA potential is the torsion interaction, which are described by the *opls* dihedral style in the simulations. The form of *opls* dihedral style is as follows,

$$E(\phi) = \frac{V_1}{2}[1+\cos(\phi)] + \frac{V_2}{2}[1-\cos(2\phi)] + \frac{V_3}{2}[1+\cos(3\phi)] \quad \text{(S6)}$$

where V_1, V_2 and V_3 are the dihedral coefficients. The detailed dihedral parameters of OPLS-AA potential can be found in **Reference S2**. [2]

1.1.2 TIP3P water model

We employ the TIP3P model to simulate the interactions between water molecules. This model is proven to be efficient and can precisely predict the structures and thermodynamic properties of the liquid water phase. It assigns the charges and LJ parameters for each atom of the water molecule. Additionally, the *harmonic* bond and angle style are utilized to describe the O-H bond and the H-O-H angle. More detailed descriptions and parameters can be found in **Reference S3**. [3]

1.2 Simulation details

In LAMMPS software, the Nose-Hoover style non-Hamiltonian equations of motion [4, 5] are used to generate positions and velocities of atoms in the simulated system from the NVT or NPT ensembles. The equations of motion used in the simulations are those of Shinoda et al. [6], which combine the hydrostatic equations of Martyna et al. [7] with the strain energy proposed by Parrinello and Rahman. [8] The time integration schemes closely follow the time-reversible measure-preserving Verlet and rRESPA integrators derived by Tuckerman et al. [9] The T_{damp} parameter deciding the speed of the relaxation of temperature is equal to 0.2 K, while the P_{damp} determining the time scale on which pressure is relaxed is a value of 1 ps. It is noteworthy that the reasonable choice for the value of P_{damp} is about 1000 timesteps. In the case of lower value of P_{damp}, pressure and volume would fluctuate severely; in the case of higher value of P_{damp}, the equilibrium for pressure would be time-consuming. In order to reduce the storage requirements for data processing, the coordinates of atoms are output every 50000 timesteps and 500 timesteps, *i.e.* 50 ps and 0.5 ps, in the NPT and NVT ensemble respectively.

Due to the strong electrostatic interactions between ions, we employ the PPPM solver to calculate the long-range Coulombic force. In this method 3d FFTs is used to solve Poisson's equation on the mesh where atom charge is mapped, and then electric fields are interpolated on the mesh points back to the atoms. The PPPM solver is a more excellent method than the Ewald summation in terms of saving the computation time and memory storage, because it scales as Nlog(N) where N is the total atom numbers while the Ewald summation scales as N^ (3/2). The accuracy of PPPM method is 0.001 eV/Å and the grid of the mesh is 18 × 18 × 27 in the simulations. In order to verify the rationality of this mesh, we further compare with different number of grid mesh, as shown in **Figure S1**. As well can see, when the number of grid mesh

equals to 18 × 18 × 27, the total, kinetic and potential energy gradually reach a steady. Although the E_coul is not completely steady, we chose the grid of mesh (18 × 18 × 27) in the simulations, which may be a little rough, to reduce computing time and improve computational efficiency.

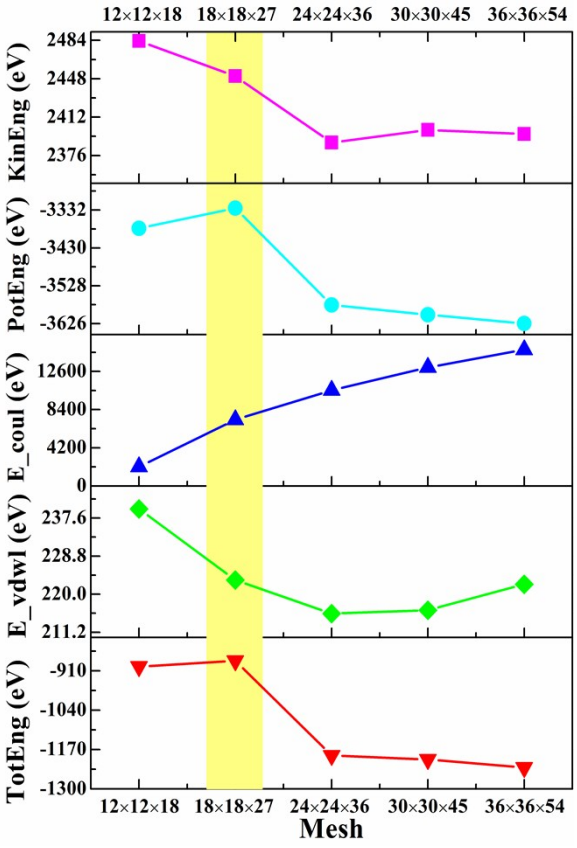

Figure S1. Variation of energies with the number of grid mesh increasing

We perform analysis of the simulation results in the NVT ensemble after running the NPT ensemble. In order to control the pressure, the values of box parameter are changed. Thus, we report the values of box parameter of all simulation cases in the NVT ensemble. **Table S3** lists all the box parameters of all simulation conditions in the NVT ensemble. With temperature increasing, the box parameters (L_x, L_y and L_z) is slightly larger due to the thermal expansion of the simulation system. Owing to the stronger hydration of divalent cations, the volume of simulation systems with Ca^{2+} or Mg^{2+} is a bit bigger. **Figure S2** shows that the L_x or L_y almost increases linearly with temperature rising for cases with different cations. We fit the curve and obtain the slopes as well as their standard error (Ca^{2+} > Mg^{2+} > Na^{+}), which we attribute to the stronger hydration of divalent cations.

Table S3. Box parameters of all cases in the NVT ensemble.

Cation	Temperature (K)	Cases	L_x	L_y	L_z
Na^+	300	Case 1_1	76.300828	76.300828	111.09942
Na^+	310	Case 1_2	76.610088	76.610088	111.54972
Na^+	320	Case 1_3	76.897436	76.897436	111.96812
Na^+	330	Case 1_4	77.147551	77.147551	112.33231
Na^+	340	Case 1_5	77.481507	77.481507	112.81857
Na^+	350	Case 1_6	77.774455	77.774455	113.24513
Ca^{2+}	300	Case 2_1	76.314243	76.314243	111.11895
Ca^{2+}	310	Case 2_2	76.608268	76.608268	111.54707
Ca^{2+}	320	Case 2_3	77.016275	77.016275	112.14116
Ca^{2+}	330	Case 2_4	77.191929	77.191929	112.39693
Ca^{2+}	340	Case 2_5	77.641835	77.641835	113.05202
Ca^{2+}	350	Case 2_6	77.756437	77.756437	113.21889
Mg^{2+}	300	Case 3_1	76.427902	76.427902	111.28445
Mg^{2+}	310	Case 3_2	76.788523	76.788523	111.80954
Mg^{2+}	320	Case 3_3	76.96745	76.96745	112.07007
Mg^{2+}	330	Case 3_4	77.329913	77.329913	112.59784
Mg^{2+}	340	Case 3_5	77.5718	77.5718	112.95005
Mg^{2+}	350	Case 3_6	77.959066	77.959066	113.51393

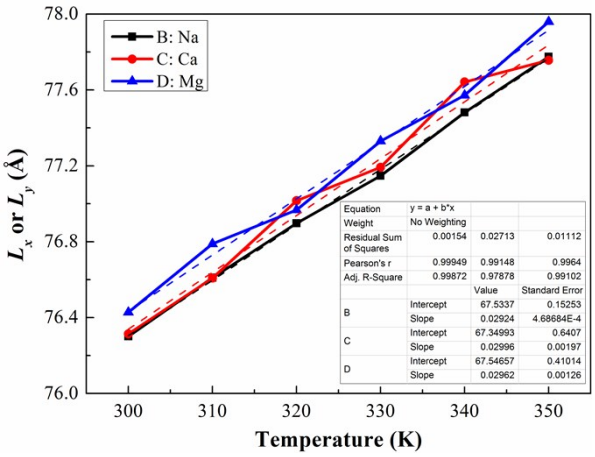

Figure S2. Variation of box parameters L_x or L_y with temperature increasing

In addition, we also analyze the average internal pressure and its relative fluctuations in the NVT simulations. Take Case 1_6 for example, we obtain the variations of pressure/temperature with simulated time, as shown in **Figure S3**. In the NVT simulations, the volume of simulation box is constant and the

temperature reaches an equilibrium value with slightly fluctuations. However, the fluctuation of pressure is great. Based on the theory of statistical mechanics, the pressure in MD simulations consists of kinetic energy term and virial term. The kinetic energy is almost constant; therefore, the great fluctuation of pressure is dominated by virial term, which is affected by interaction between molecules. Another possible reason for the great fluctuation of pressure is the limited time and space scales, which are decided by molecular relaxation time and free path. Although the fluctuation of pressure is great, time-averaged pressure of our simulation systems (1-2 bar) is a little bigger than desired pressure (1.01325 bar) controlled by the NPT ensemble. We attribute to the not long enough simulation time and enough space.

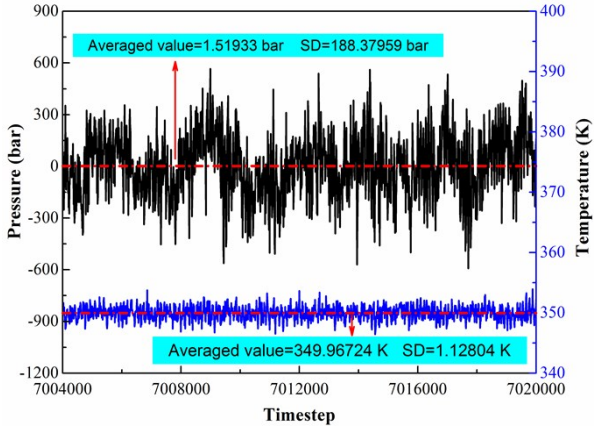

Figure S3. Variation of temperature and pressure *versus* timestep

1.3 Model validation

In our previous work, [10] we made a detailed validation of our simulation model by comparing the simulated bulk densities or interfacial tension (IFT) with the actual value of them under the same conditions. The results show that our simulation model and methods for decane-water-ions systems are reasonable and feasible. In this paper, silica nanoparticles are added in the decane-water-ions systems. The potential parameters of silica NPs used in our work have been proven to be effective and the simulation results based on them are consistent with experimental results. [11] In addition, we obtain the simulated averaged IFT value during the equilibrium processes (see **Figure S4**) and compare the simulated IFT of decane-water-NPs-ions systems with other results from simulations or experiments.[12-16] Considering that the differences of the conditions (temperature, pressure, ionic concentration and particle size) between the

simulations and the literatures, our results are close to other results, proving the feasibility and efficiency of our model and methods.

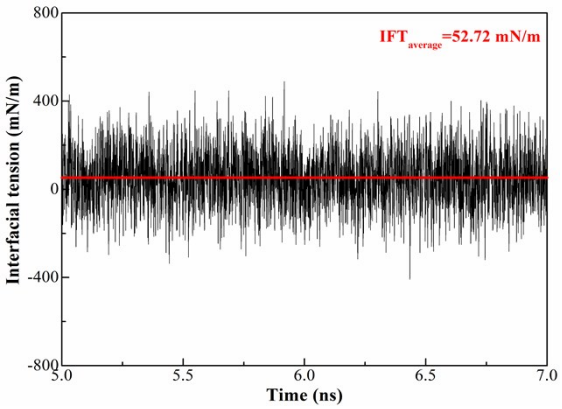

Figure S4. Averaged IFT of Case 1_1 during the equilibrium process

2. Interfacial structure

2.1 Interfacial thickness

As stated in the manuscript, we can obtain the interfacial thickness of the decane-water-NPs systems with different cations (300 K, 1 atm), as shown in **Figure S5**. For cases without NPs, the addition of ions causes a slight decrease of the interfacial thickness due to the ionic hydration. After adding NPs, the interfacial thickness enlarges. Meanwhile, the effects of ions on the interfacial thickness are different from those cases without NPs. The order of interfacial thickness is as follows: $Na^+ > Ca^{2+} > Mg^{2+}$. We attribute those phenomena to the large size of NPs (r = 7.5 Å) and the interaction between NPs/ions.

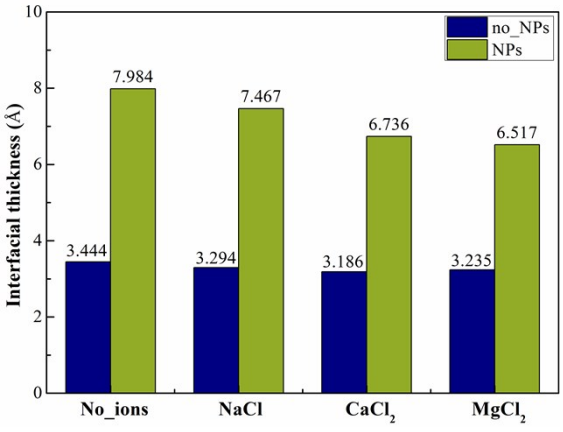

Figure S5. Interfacial thickness *vs.* ion species under 300 K, 1 atm condition

2.2 Density distribution of ions

Figure S6 shows the number density of cations along *z*-direction for cases under 300 K, 1 atm condition. Compared to sodium ions, calcium and magnesium ions have greater number density near the interfacial zone, indicating that calcium and magnesium ions are likely to appear near the interface. Therefore, more water molecules would be attracted by cations and leave the interfacial zone, resulting in a slight decrease of the interfacial thickness, which can be seen from **Figure S5**. Particularly, the fluctuation of curves in **Figure S6** is probably because the ionic hydration hinders the motion of ions or the total simulated time is not long enough. The fluctuation of curves for Ca^{2+} or Mg^{2+} is severer than that of curve for Na^{+} due to their stronger hydration.

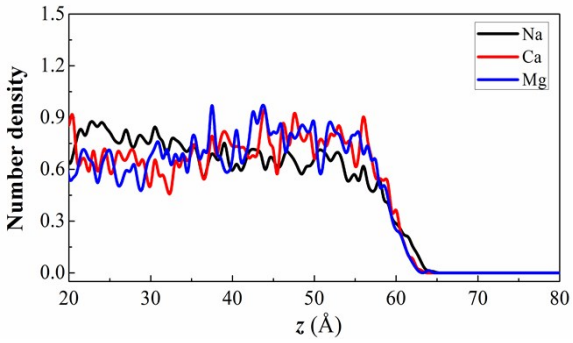

Figure S6. Number density distribution of cations along *z*-direction for cases under 300 K, 1 atm condition

2.3 Hydration number of ions

In order to achieve the density distribution (RDF) *g*(r), it is necessary to obtain the number of atoms at each layer $\langle \Delta N_{ij,n} \rangle$ and the *n*(*r*) function along radial direction, as shown in **Figure S7**. The positions where the $\langle \Delta N_{ij,n} \rangle$ curves reach a peak for Mg^{2+} is smaller than those for Na^{+} and Ca^{2+}, meaning that the Mg^{2+} has smallest radius of hydration. Meanwhile, due to the stronger hydration of divalent cations (Ca^{2+} and Mg^{2+}), the second peak of curves is more obvious. The *n*(*r*) function, which is the integral of the *g*(*r*), increases with the distance *r* rising. There are two obviously risen stage when the *g*(*r*) reaches the peaks. Based on these curves, we can further achieve the number of hydration for Na^{+}, Ca^{2+} and Mg^{2+}, which approximately equal to 5.2, 7.4 and 6.7 respectively. These results are close to the results in the literatures. [17-22] It also reflects the accuracy of the potential models which we used in the simulations.

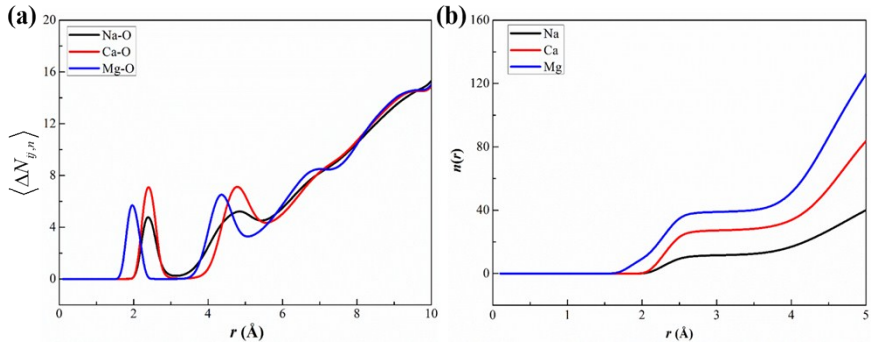

Figure S7. Number of atoms at the layer $\langle \Delta N_{ij,n} \rangle$ and the $n(r)$ function along the radial direction

3. Dynamics of nanoparticles

3.1 Calculation of diffusion coefficient

In order to obtain the diffusion coefficients of nanoparticles at the interface, we adopt the Einstein equation, as follows:

$$D = \frac{\left\langle (x - x_0)^2 + (y - y_0)^2 + (z - z_0)^2 \right\rangle}{6\Delta t} \tag{S7}$$

where x_0, y_0 and z_0 are the initial coordinates at $t = 0$, Δt is the time interval for nanoparticles moving from (x_0, y_0, z_0) to (x, y, z), D is diffusion coefficient and numerator means the mean-square-displacement (MSD).

Figure S8 shows the time-averaged MSD of nanoparticles (Case 1_1) within 5 ns simulation time. Because of few nanoparticles (two) in our simulations, the fluctuation of MSD curves is severe. We only fit the slope of yellow-part line and acquire the interfacial diffusion coefficient.

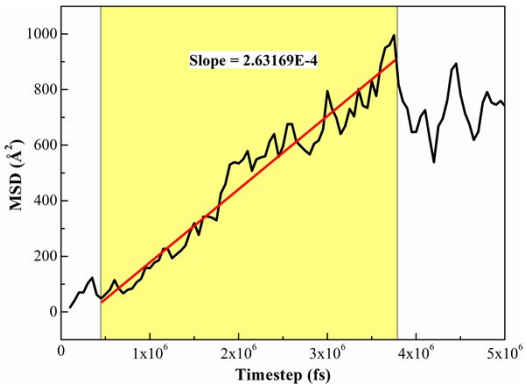

Figure S8. MSD of nanoparticles *versus* time

References

1. G. Kaminski, E. M. Duffy, T. Matsui and W. L. Jorgensen, *J. Phys. Chem.*, 1994, **98**, 13077-13082.
2. S. W. I. Siu, K. Pluhackova and R. A. Böckmann, *J. Chem. Theory Comput.*, 2012, **8**, 1459-1470.
3. W. L. Jorgensen, J. Chandrasekhar, J. D. Madura, R. W. Impey and M. L. Klein, *J. Chem. Phys.*, 1983, **79**, 926-935.
4. S. Nosé, *Mol. Phys.*, 1984, **52**, 255-268.
5. W. G. Hoover, *Phys. Rev. A Gen. Phys.*, 1985, **31**, 1695-1697.
6. W. Shinoda, M. Shiga and M. Mikami, *Phys. Rev. B*, 2004, **69**, 134103.
7. G. J. Martyna, D. J. Tobias and M. L. Klein, *J. Chem. Phys.*, 1994, **101**, 4177-4189.
8. M. Parrinello and A. Rahman, *Phys. Rev. Lett.*, 1980, **45**, 1196-1199.
9. M. E. Tuckerman, J. Alejandre, R. López-Rendón, A. L. Jochim and G. J. Martyna, *J. Phys. A Gen. Phys.*, 2006, **39**, 5629.
10. B. Wen, C. Sun, B. Bai, E. Y. Gatapova and O. A. Kabov, *Phys. Chem. Chem. Phys.*, 2017, **19**, 14606-14614.
11. F. S. Emami, V. Puddu, R. J. Berry, V. Varshney, S. V. Patwardhan, C. C. Perry and H. Heinz, *Chem. Mater.*, 2014, **26**, 2647-2658.
12. C. O. Metin, J. R. Baran, Jr. and Q. P. Nguyen, *J. Nanopar. Res.*, 2012, **14**, 1246.
13. S. Ferdous, M. A. Ioannidis and D. E. Henneke, *J. Nanopar. Res.*, 2012, **14**, 850.
14. L. S. de Lara, M. F. Michelon, C. O. Metin, Q. P. Nguyen and C. R. Miranda, *J. Chem. Phys.*, 2012, **136**, 164702.
15. M. A. Fernandez-Rodriguez, J. Ramos, L. Isa, M. A. Rodriguez-Valverde, M. A. Cabrerizo-Vilchez and R. Hidalgo-Alvarez, *Langmuir*, 2015, **31**, 8818-8823.
16. H. Fan, D. E. Resasco and A. Striolo, *Langmuir*, 2011, **27**, 5264-5274.
17. S. B. Rempe and L. R. Pratt, *Fluid Phase Equil.*, 2001, **183**, 121-132.
18. I. Bakó, J. Hutter and G. Pálinkás, *J. Chem. Phys.*, 2002, **117**, 9838-9843.
19. A. L. V. Geet, *J. Am. Chem. Soc.*, 1972, 5583-5587.
20. RiahiSaleh, RouxBenoît and N. Rowleychristopher, *Can. J. Chem.*, 2013, **91**, 552-558.
21. J. Mähler and I. Persson, *Inorg. Chem.*, 2012, **51**, 425-438.
22. G. Bai, H.-B. Yi, H.-J. Li and J.-J. Xu, *Mol. Phys.*, 2013, **111**, 553-568.